Effect of adding copper oxide nanoparticles on the mass/heat transfer in falling film absorption

GAO Hongtao[a*], MAO Fei[a], SONG Yuchao[a], HONG Jiaju[a], YAN Yuying[b]

a *Institute of Refrigeration & Cryogenics Engineering, Dalian Maritime University, 116026, Dalian, China*

b *Fluids & Thermal Engineering Research Group, Faculty of Engineering, University of Nottingham, University Park, Nottingham NG7 2RD, UK*

**Corresponding author: Dr. GAO Hongtao; Email: gaohongtao@dlmu.edu.cn*

Abstract

Absorber is an essential component that affects the efficiency of absorption refrigeration unit. Falling film absorption is one of the most widespread forms of the heat/mass transfer in absorption system. In this paper, based on the software COMSOL Multiphysics, the finite element method is used to establish the model of falling film absorption. The falling film absorption properties of nanofluids was studied by adding CuO nanoparticles. The results reveal that as the film flow rate increases, the average mass transfer flux rises first and then decreases. The average mass transfer flux increases with the rise of the concentration of solution at the inlet, the decrease of the temperature of solution at the inlet and the reduction of cooling water inlet temperature. After adding copper oxide nanoparticles to lithium bromide solution, the vapor absorption performance of lithium bromide solution can be significantly improved.

Keywords

Falling film absorption; Mass transfer; Heat transfer; Lithium bromide; Nanoparticles; Numerical study.

Nomenclature

C	mass concentration, %
c_p	specific heat at constant pressure, $J \cdot kg^{-1} \cdot K^{-1}$
D	diffusion coefficient, $m^2 \cdot s^{-1}$
g	gravitational acceleration, $m \cdot s^{-2}$
H_{abs}	heat of absorption, $kJ \cdot kg^{-1}$
k	thermal conductivity, $W \cdot m^{-1} \cdot K^{-1}$
L	falling film length, m
h_m	mass transfer coefficient, $m \cdot s^{-1}$
m	Mass transfer flux, $kg \cdot m^{-2} \cdot s^{-1}$
M	mass transfer rate, $kg \cdot m^{-1} \cdot s^{-1}$
P	pressure, kPa
q	heat transfer flux, $kW \cdot m^{-2}$
Q	heat transfer rate, $W \cdot m^{-1}$
T	temperature, K
u	velocity in x-direction, $m \cdot s^{-1}$
v	velocity in y-direction, $m \cdot s^{-1}$
Re	Reynolds number
x	coordinate of flow direction， m
y	coordinate perpendicular to the direction of flow， m
δ_0	liquid film thickness, m

u_{mean}	average flow velocity，m·s^{-1}
μ	dynamic viscosity, Pa·s
ρ	density, kg·m^{-3}
Γ	film flow rate, kg·m^{-1}·s^{-1}
Φ	volume fraction of nanoparticles
R	mass transfer enhancement factor
ϕ_{ext}^{21}	Extrapolated values
e_a^{21}	Approximate relative error
e_{ext}^{21}	Extrapolated relative error
GCI_{fine}^{21}	Fine-grid convergence index
p	Apparent order of the method
r	Mesh refinement ratio
s	Signum function

Subscripts

nf	nanofluid
c	cooling water
Cu	copper
n	nanoparticle
f	fluid
abs	absorption
in	inlet
out	outlet
w	wall

i liquid-vapor interface

1. Introduction

The research of absorption refrigeration technology has attracted many scholars' attention. Improving the heat/mass transfer is the most effective mean to enhance the efficiency of the absorber. Adding nanoparticles is one of the means to effectively improve the performance of the absorber [1-2]. Many scholars have investigated the effects of nanoparticles on the performance of absorbers through experimental methods. Pang et al. [3], Khan and Gorla [4] and Chen et al. [5] concluded that the performance of absorbers could be improved by adding nanoparticles. Heris et al. [6] investigated the influences of adding CuO and Al_2O_3 nanoparticles on the properties of laminar falling film absorption under the condition of constant temperature wall. They found that the heat transfer coefficient rose with increasing concentration of nanoparticles. The influence of nanoparticles on the mass/heat transfer mainly depended on thermal conductivity, chaotic movements, fluctuations and interactions. Kang et al. [7] studied the absorption process of binary nanofluids with iron nanoparticles and carbon nanotubes. The results showed that the improvement of carbon nanotubes was more obvious, and the improvement in mass transfer is more pronounced than in heat transfer in binary nanofluids. Kim et al. [8] investigated the performance of bubble absorption in nanofluids. It was determined that the absorption performance with nanoparticles increased by 3.21 times. For the solution with lower absorption capacity, the enhancement effect of nanoparticles was more prominent. Yang et al. [9] studied the influence of Fe_2O_3 and $ZnFe_2O_4$ nanoparticles on the performance of the absorber. They observed that the effective absorption of Fe_2O_3 and $ZnFe_2O_4$ nanofluids was increased by 70% and 50%, respectively, when the initial ammonia mass fraction was 15%. It was concluded that the enhancement of absorption was due to the decrease of viscosity of nanofluids. Li et al. [10] presented a falling film generating test bench for testing ammonia vapor generation rate with/without

nanoparticles. The enhancement mechanism was analyzed from the micro-motion, interface effect, Marangoni effect and physical properties of nanofluids. Their result indicated that the micro-motion of nanofluids and the physical properties were the two main factors of the enhancement of falling film by nanofluids.

Some scholars have discussed the influence of nanoparticles on the performance of the absorber by numerical simulation. Armou et al. [11] established a CFD model for falling film absorption of nanofluids in laminar flow based on the assumption that the wall temperature changes linearly. The numerical results revealed that nanofluids have higher mass transfer capacity. The heat/mass transfer performance of binary nanofluids was more potent than that of pure lithium bromide solution. Wang et al. [12] simulated the absorption properties of nanofluids on inclined plates assuming that the physical properties of LiBr solution and the wall temperature were constant. Their results revealed that nanofluids have a higher water vapor absorption rate than pure solutions. When the flow rate was $1.0\ \mathrm{L \cdot min^{-1}}$, the mass transfer coefficients of 0.05% and 0.1% nanofluids increased 1.28 and 1.41 times, respectively. Zhang et al. [13] established a CFD model for describing the falling film absorption process based on the assumption of constant wall temperature, consisted of Fe_3O_4 nanoparticles and LiBr solution. They found that the higher the concentration of nanoparticles or the smaller the size of nanoparticles, the stronger the heat transfer and mass transfer. Moghadassi et al. [14] established a CFD model for the absorption outside a horizontal circular tube under the boundary conditions of constant wall heat flux, and added 0.1% Al_2O_3 and Al_2O_3-Cu nanoparticles to study the influence of nanoparticles on the heat transfer. They found that the convective heat transfer coefficient of nanofluids was higher. Khanolkar and Suresh [15] investigated the effect of Silica and Titanium dioxide nanofluids on the mass transfer rate by experimental and theoretical methods. When the volume fraction of nanoparticle is small, the mass transfer coefficient can be increased by 165%. Some scholars have also investigated the hydrodynamic characteristics of falling film absorption. Karami et al. [16] investigated the falling film absorption with Reynolds numbers of 5 to 150, and assumed the flow state

of being laminar. The simulation results agree well with the experimental data. However, for higher Reynolds numbers, waves (capillary waves, inertial waves, etc.) will appear in the flow and affect the mass transfer. The falling film flow can no longer be assumed to be laminar.

Some scholars have found other ways to enhance the performance of falling film absorption. Gao et al. [17] added alcoholic surfactants with different carbon atom numbers into lithium bromide solution. It was found that the lower the surface tension, the better the mass transfer ability of lithium bromide solution. Niu et al.[18] established a model of ammonia water to absorb water vapor in a magnetic field. It was determined that the magnetic field had a significant improvement on the absorption of water vapor by ammonia water.

The performance of binary fluid falling film absorption has been discussed in many experimental and theoretical literatures. Although a lot of work has been done in the numerical study of binary fluid falling film absorption, there is still a lack of complete numerical simulation for falling film absorption considering actual cooling water channels and tube wall thickness. Based on the software COMSOL Multiphysics, the finite element method is used to investigate the vertical falling film absorption. In order to make the model closer to reality, the actual cooling water channel and the tube wall thickness was considered, and the change of solution physical properties was also considered. The effect of adding copper oxide nanoparticles on the performance of falling film absorption was investigated.

2. Mathematical physics model

2.1 Physical model

Fig. 1 depicts the 2D model of the absorption process. The solution at the inlet is sprayed onto the wall. Due to gravity, the solution flows down along the inner wall of the absorber and it begins to absorb water vapor, while releasing absorbed heat, which causes the temperature of film to rise. On the outside of the wall, there is a countercurrent upward cooling water to cool the solution, ensuring

the absorption process going continuously. In order to establish a physical and mathematical model reflecting the actual absorption process and convenient for analysis and comparison, the model is assumed as follows.

(1) Falling film flow is a fully developed laminar flow.

(2) The CuO nanoparticles are evenly dispersed in the LiBr aqueous solution.

(3) The film thickness is constant.

(4) The solution is in phase equilibrium at the inlet and at the vapor-liquid interface.

(5) The heat transfer to the water vapor phase is negligible.

2.2 Governing equations

According to the above basic assumptions mentioned above, the basic governing equation of the solution area is as follows:

$$\frac{\partial}{\partial x}(\rho_{\mathrm{nf}}u)+\frac{\partial}{\partial y}(\rho_{\mathrm{nf}}v)=0 \tag{1}$$

$$\frac{\partial(\rho_{\mathrm{nf}}uu)}{\partial x}+\frac{\partial(\rho_{\mathrm{nf}}vu)}{\partial y}=\frac{\partial}{\partial x}\left(\mu_{\mathrm{nf}}\frac{\partial u}{\partial x}\right)+\frac{\partial}{\partial y}\left(\mu_{\mathrm{nf}}\frac{\partial u}{\partial y}\right)+\rho_{\mathrm{nf}}g \tag{2}$$

$$\frac{\partial(\rho_{\mathrm{nf}}uv)}{\partial x}+\frac{\partial(\rho_{\mathrm{nf}}vv)}{\partial y}=\frac{\partial}{\partial x}\left(\mu_{\mathrm{nf}}\frac{\partial v}{\partial x}\right)+\frac{\partial}{\partial y}\left(\mu_{\mathrm{nf}}\frac{\partial v}{\partial y}\right) \tag{3}$$

$$u\frac{\partial\left((\rho c_{\mathrm{p}})_{\mathrm{nf}}T_{\mathrm{nf}}\right)}{\partial \mathrm{x}}+v\frac{\partial\left((\rho c_{\mathrm{p}})_{\mathrm{nf}}T_{\mathrm{nf}}\right)}{\partial \mathrm{y}}=\frac{\partial}{\partial \mathrm{x}}\left(k_{\mathrm{nf}}\frac{\partial T_{\mathrm{nf}}}{\partial \mathrm{x}}\right)+\frac{\partial}{\partial \mathrm{y}}\left(k_{\mathrm{nf}}\frac{\partial T_{\mathrm{nf}}}{\partial \mathrm{y}}\right)+\frac{\partial}{\partial \mathrm{y}}(mH_{\mathrm{abs}}) \tag{4}$$

$$\frac{\partial(\rho_{\mathrm{nf}}uC)}{\partial \mathrm{x}}+\frac{\partial(\rho_{\mathrm{nf}}vC)}{\partial \mathrm{y}}=\frac{\partial}{\partial \mathrm{x}}\left(\rho_{\mathrm{nf}}D\frac{\partial C}{\partial \mathrm{x}}\right)+\frac{\partial}{\partial \mathrm{y}}\left(\rho_{\mathrm{nf}}D\frac{\partial C}{\partial \mathrm{y}}\right) \tag{5}$$

The basic governing equation of the copper tube area is as follows:

$$\frac{\partial^2 T_{\mathrm{Cu}}}{\partial x^2}+\frac{\partial^2 T_{\mathrm{Cu}}}{\partial y^2}=0 \tag{6}$$

The basic governing equation of the cooling water area is as follows:

$$\frac{\partial}{\partial x}(\rho_{\mathrm{c}}u)+\frac{\partial}{\partial y}(\rho_{\mathrm{c}}v)=0 \tag{7}$$

$$\frac{\partial(\rho_{\mathrm{c}}uu)}{\partial x}+\frac{\partial(\rho_{\mathrm{c}}vu)}{\partial y}=\frac{\partial}{\partial x}\left(\mu_{\mathrm{c}}\frac{\partial u}{\partial x}\right)+\frac{\partial}{\partial y}\left(\mu_{\mathrm{c}}\frac{\partial u}{\partial y}\right)+\rho_{\mathrm{c}}g \tag{8}$$

$$\frac{\partial(\rho_{\mathrm{c}} uv)}{\partial x}+\frac{\partial(\rho_{\mathrm{c}} vv)}{\partial y}=\frac{\partial}{\partial x}\left(\mu_{\mathrm{c}} \frac{\partial v}{\partial x}\right)+\frac{\partial}{\partial y}\left(\mu_{\mathrm{c}} \frac{\partial v}{\partial y}\right) \tag{9}$$

$$u \frac{\partial\left(\left(\rho c_{\mathrm{p}}\right)_{\mathrm{c}} T_{\mathrm{c}}\right)}{\partial \mathrm{x}}+v \frac{\partial\left(\left(\rho c_{\mathrm{p}}\right)_{\mathrm{c}} T_{\mathrm{c}}\right)}{\partial \mathrm{y}}=\frac{\partial}{\partial \mathrm{x}}\left(k_{\mathrm{c}} \frac{\partial T_{\mathrm{c}}}{\partial \mathrm{x}}\right)+\frac{\partial}{\partial \mathrm{y}}\left(k_{\mathrm{c}} \frac{\partial T_{\mathrm{c}}}{\partial \mathrm{y}}\right) \tag{10}$$

2.3 Boundary conditions

(1) At the solution inlet, the solution in phase equilibrium.

$$x=0; T=T_{\mathrm{in}}; C=C_{\mathrm{in}} \tag{11}$$

(2) The boundary conditions at solution outlet are as follows:

$$x=L; \frac{\partial T}{\partial x}=0; \frac{\partial C}{\partial x}=0 \tag{12}$$

(3) The boundary conditions at the liquid-vapor interface are as follows:

$$C_i=C_i(P, T) \tag{13}$$

$$m=-\rho D\left(\frac{\partial C}{\partial y}\right)_{y=\delta_0} \tag{14}$$

(4) At the cooling water inlet, the temperature is evenly distributed.

$$x=L; T=T_{\mathrm{c,in}} \tag{15}$$

(5) At the cooling water outlet, the flow is in fully developed state.

$$x=0; \frac{\partial T}{\partial x}=0 \tag{16}$$

In order to give an intuitive impression, the boundary conditions and geometric details are also shown in Figure 2.

2.4 Related parameters

The formula for the film Reynolds number is as follows [19]:

$$Re=\frac{4\Gamma}{\mu_{\mathrm{nf}}} \tag{17}$$

The film thickness is defined by Nusselt's analysis.

$$\delta_0 = \left(\frac{3\Gamma\mu_{\mathrm{nf}}}{\rho_{\mathrm{nf}}{}^2 g}\right)^{\frac{1}{3}} \tag{18}$$

According to the Nusselt theory, the velocity profile is as follows:

$$u = \frac{3}{2}u_{\mathrm{mean}}\left[2\frac{y}{\delta_0} - \left(\frac{y}{\delta_0}\right)^2\right] \tag{19}$$

where $u_{\mathrm{mean}} = \frac{\Gamma}{\rho_{\mathrm{nf}}\delta_0}$

2.5 Nanofluid properties

The density, the dynamic viscosity, the specific heat and the thermal conductivity of the nanofluid is respectively determined by the followings [20-22]:

$$\rho_{\mathrm{nf}} = (1-\Phi)\rho_{\mathrm{f}} + \Phi\rho_{\mathrm{n}} \tag{20}$$

$$\mu_{\mathrm{nf}} = \frac{\mu_{\mathrm{f}}}{(1-\Phi)^{2.5}} \tag{21}$$

$$(\rho c_{\mathrm{P}})_{\mathrm{nf}} = (1-\Phi)(\rho c_{\mathrm{P}})_{\mathrm{f}} + \Phi(\rho c_{\mathrm{P}})_{\mathrm{n}} \tag{22}$$

$$\frac{k_{\mathrm{nf}}}{k_{\mathrm{f}}} = \frac{k_{\mathrm{n}}+2k_{\mathrm{f}}-2\Phi(k_{\mathrm{f}}-k_{\mathrm{n}})}{k_{\mathrm{n}}+2k_{\mathrm{f}}+\Phi(k_{\mathrm{f}}-k_{\mathrm{n}})} \tag{23}$$

3 Numerical procedure

3.1 Solution method and meshing

The laminar flow, physics transport of concentrated species and heat transfer in fluids are selected in COMSOL Multiphysics to establish a two-dimensional absorption model for a falling film of LiBr solution flowing along a vertical wall of copper with length of 150 mm, thickness of 1 mm. Steady-state, PAEDISO solver and a preordering algorithm of nested dissection multithread are adopted. A structured quadrilateral mesh compatible with the calculation area is used in the model.

As listed in Table 1, the mesh sensitivity is estimated with three different numbers of meshes (fine, medium, and coarse). The mesh convergence ratio R_G is expressed as follows:

$$R_G = \frac{\varepsilon_{21}}{\varepsilon_{32}} \tag{24}$$

where $\varepsilon_{32} = \phi_3 - \phi_2$, $\varepsilon_{21} = \phi_2 - \phi_1$, and ϕ_k denotes the solution on the k^{th} mesh. It can be observed from the Table 2 that the state of mesh is convergent.

The Grid Convergence Method (GCI) method is used for discretization error estimation in this paper [23]. The parameters of discretization error, such as the apparent order of the method p, the extrapolated values ϕ_{ext}^{21}, the approximate relative error e_a^{21}, the extrapolated relative error e_{ext}^{21}, and the fine-grid convergence index GCI_{fine}^{21}, are defined as follows:

$$p = \frac{1}{\ln(r_{21})}\left|\ln\left|\varepsilon_{32}/\varepsilon_{21}\right| + q(p)\right| \tag{25}$$

$$q(p) = \ln\left(\frac{r_{21}^p - s}{r_{32}^p - s}\right) \tag{26}$$

$$\phi_{ext}^{21} = \left(r_{21}^p \phi_1 - \phi_2\right)/\left(r_{21}^p - 1\right) \tag{27}$$

$$e_a^{21} = \left|\frac{\phi_1 - \phi_2}{\phi_1}\right| \tag{28}$$

$$e_{ext}^{21} = \left|\frac{\phi_{ext}^{21} - \phi_1}{\phi_{ext}^{21}}\right| \tag{29}$$

$$GCI_{fine}^{21} = \frac{1.25 e_a^{21}}{r_{21}^p - 1} \tag{30}$$

where r is the mesh refinement ratio, and $s = 1 \cdot \mathrm{sgn}\left(\varepsilon_{32}/\varepsilon_{21}\right)$ is signum function. It can be seen from table 3 that for the mass transfer flux, the numerical uncertainties in the fine-mesh solution is 0.018%, which meets the requirements of numerical simulation. Simultaneously, the mass transfer flux are calculated using 9 various grids, as shown in Figure 3. The deviation of mass transfer flux between the grid of 135000 and the grid of 180000 is only 0.03%, so the grid of 135000, being enough to meet the calculation requirements, is selected in this simulation investigation.

3.2 Model validation

Under the same operating conditions (0.1% CuO nanoparticles added), our numerical results are compared with the experimental result of Wang et al [12], as shown in Figure 4, which shows the change of outlet concentration of the absorber with flowing rate of nano-LiBr aqueous solution. It can be seen that the two are basically the same, and the maximum deviation is not more than 0.7%.

The parameters of operating conditions used in the calculation of the present study are shown in Table 4.

4 Results and discussion

4.1 Mass transfer flux at the interface

The influence of the concentration of nano-copper oxide on the absorption properties was mainly studied. Figure 5 shows the effect of nanoparticles with increasing volume fraction on mass transfer flux. When no nanoparticle is added ($\Phi = 0$), the mass transfer flux rises rapidly within 50 mm of the inlet and reaches the maximum value ($\mathrm{m_{i,max}} = 2.2 \times 10^{-3}\ kg \cdot m^{-2} \cdot s^{-1}$), then begins to decline. Since the solution is in phase equilibrium at the inlet, when x=0, the mass transfer driving force is 0, and the mass transfer flux is 0. When the solution enters the tube, the cooling effect quickly reaches the interface, reducing the temperature of the interface, and decreasing the saturated vapor pressure of lithium bromide aqueous solution, and then increasing the mass transfer driving force and therefore increases the mass transfer flux at the interface. However, as the absorbed water vapor gradually increases, the latent heat released gradually increases, which causes the temperature of the interface to grow, the saturation pressure of the solution to grow, and the mass transfer flux to reduce. Simultaneously, as the downstream distance increases, lithium bromide solution has absorbed more water vapor, which leads to the decrease of water vapor absorption capacity of the solution, so the mass transfer flux decreases.

In this paper, it is assumed that the CuO nanoparticles are evenly dispersed in the LiBr aqueous solution. Thence, in the numerical investigation, only the low volume fraction of nanoparticles is investigated. As more nano-copper oxide is added, the mass transfer flux increases, and the trends of the five curves are consistent. The effect of the nanoparticles is not obvious near the inlet. It can be derived that the steam partial pressure difference between interface and water vapor is quite big at the inlet, driving the water vapor to go into the interface. And this plays a leading role in the initial stage, making the impact from the nanoparticles insignificant. When the falling film length is 50 mm, the mass transfer flux of the lithium bromide solution containing 0.1% nanoparticles is 1.36 times that of the pure solution. This is because the irregular Brownian motion of nano-copper oxide makes the mass diffusion coefficient increase. At the same time, the concentration of water in the lithium bromide aqueous solution with copper oxide nanoparticles is slightly lower, that is, the partial pressure of water vapor is slightly lower than that of the pure solution. The driving force for mass transfer (water vapor partial pressure difference) is increased. Therefore, as the volume fraction of nano-copper oxide increases, the mass transfer flux increases.

4.2 Variation of mass transfer coefficient and mass transfer rate in the liquid phase

The formula for calculating the liquid mass transfer coefficient is as follows:

$$h_m(x) = \frac{m(x)}{\rho(C_{\mathrm{w}}(x) - C_{\mathrm{i}}(x))} \tag{31}$$

Figure 6 shows the relationship between the liquid-phase mass transfer coefficient and the concentration of nano-copper oxide. When no nanoparticles are added, the liquid mass transfer coefficient reaches the maximum near the inlet ($h_{\mathrm{m,max}} = 1.45 \times 10^{-4}\ m \cdot s^{-1}$), but with the increase of downstream distance, the liquid mass transfer coefficient reduces rapidly and then stabilizes. The reason can be explained that with the absorption of water vapor, the concentration of LiBr in the film becomes lower, and the partial pressure of water vapor becomes larger, resulting in a decrease in the

driving force for mass transfer.

A small amount of nanoparticles has a positive effect on the liquid phase mass transfer coefficient (Fig. 6). The liquid phase mass transfer coefficient of LiBr solution with 0.1% nanoparticles at the outlet is 1.59 times higher than that of pure solution. This is because the perturbation of the nanoparticles enhances mass transfer.

Fig. 7 depicts the relationship between the mass transfer rate and the downstream distance. The mass transfer rate rises with increase in the downstream distance. As the concentration of nano-copper oxide increases, the mass transfer rate increases, but near the inlet, the role of the nanoparticles is not significant.

4.3 Effect of film flow rate of solution

The mass transfer enhancement factor (R) is defined as the ratio of the mass transfer flux of the nanofluids to the mass transfer flux of pure lithium bromide solution under the same conditions. The coefficient can be expressed as:

$$R = \frac{m_{\mathrm{nf}}}{m_{\mathrm{f}}} \tag{32}$$

Figure 8(a) shows the influence of the concentration of nano-copper oxide on the average mass transfer flux as a function of film flow rate. When the volume fraction of nano-copper oxide volume fraction is Φ=0, as the film flow rate rises, the average mass transfer flux first rises and then decreases. When the film flow rate is $0.05\ kg \cdot m^{-1} \cdot s^{-1}$, the average mass transfer flux reaches the maximum ($m_{\mathrm{avg}} = 2.34 \times 10^{-3}\ kg \cdot m^{-2} \cdot s^{-1}$). This is because with the increase of the film flow rate, the LiBr solution is renewed faster, the absorption capacity is enhanced, and more water vapor can be absorbed, so that the average mass transfer flux is increased. As the film flow rate continues to increase to a certain extent, the liquid film renews too quickly, which shortens the time for water vapor to contact the liquid film, which results in a decrease in water vapor absorption and a decrease in average mass

transfer flux. Therefore, the average mass transfer flux does not always increase with the rise of the film flow rate, and the excessive or small flow rate is not conducive to the absorption process.

As the volume fraction of nano-copper oxide increases, the average mass transfer flux is improved. From the data of mass transfer enhancement factor shown in Figure 8(b) as a function of film flow rate and the volume fraction of nano-copper oxide, the effect of nanoparticle addition on mass transfer flux can be analyzed in more detail. At low film flow rates, the increase of average mass transfer flux by nanoparticles is not obvious. The average mass transfer flux increased by 1.24 times with the addition of 0.1% nanoparticles at the flow rate of $0.01\ kg \cdot m^{-1} \cdot s^{-1}$. With the increase of the flow rate, the mass transfer enhancement factor tends to increase slowly. The average mass transfer flux with 0.1% nanoparticles is 1.41 times higher than that of the pure lithium bromide solution at the flow rate of $0.05\ kg \cdot m^{-1} \cdot s^{-1}$.

4.4 Effect of the temperature of solution at the inlet

As the inlet temperature of the solution increases, the influence of the concentration of the nano-copper oxide on the average mass transfer flux is shown in Figure 9(a). When no nanoparticles are added, the increase of the temperature of solution at the inlet has a negative effect on mass transfer flux. The inlet temperature increases from 313.15 K to 333.15 K, the average mass transfer flux decreases 22%. This is considered that the water vapor pressure of lithium bromide solution rises with the increase of the temperature of solution at the inlet, which leads to the decrease of mass transfer driving force.

As the concentration of nanoparticles increases, the average mass transfer flux increases, and the five curves with different volume fractions have the same trend. Figure 9(b) shows the influence of nanoparticles on the mass transfer enhancement factor with increasing inlet temperature. When the temperature at the inlet increases from 313.15 K to 333.15 K, the mass transfer enhancement factor of lithium bromide solution with 0.1% nanoparticles increases from 1.32 to 1.36, meaning with 1.32 to

1.36 times mass transfer flux of pure lithium bromide solution. Increased inlet temperature makes the role of nanoparticles more pronounced.

4.5 Effect of the concentration of solution at the inlet

Figures 10(a) and 10(b) show the effect of volume fraction of nano-copper oxide on average mass transfer flux and mass transfer enhancement factor, respectively, as the solution inlet concentration rises. Increasing the solution inlet concentration helps to increase the mass transfer flux (Figure 10(a)). When $\Phi = 0$, the average mass transfer flux increases 1.75 times as the inlet concentration increases from 60% to 70%. The higher the inlet concentration, the lower the vapor pressure of the lithium bromide solution. Therefore, the mass transfer flux increases.

As the concentration of nano-copper oxide rises from $\Phi = 0$ to $\Phi = 0.001$, the average mass transfer flux increases. When the concentration of the solution inlet is 60% and 70%, the average mass transfer fluxes are increased to 1.32 times and 1.28 times, respectively, with 0.1% of the nanoparticles. When the solution inlet concentration at the inlet is low, the enhancement of nano-copper oxide is more obvious.

4.6 Effect of the temperature of cooling water at the inlet

Figures 11(a) and 11(b) reveal the influence of CuO nanoparticles on average mass transfer flux and mass transfer enhancement factor, respectively, as the temperature of cooling water at the inlet increases. From Figure 11(a), it can be concluded that lowering the temperature of cooling water at the inlet is beneficial to the mass transfer process. When $\Phi = 0$, the cooling water inlet temperature decreases from 307.15 K to 301.15 K, the average mass transfer flux increases to 1.55 times. This is because as the temperature of cooling water at the inlet decreases, the heat transfer rate increases, resulting in a decrease in the water vapor partial pressure of the lithium bromide solution. Therefore, the mass transfer flux increases.

The average mass transfer flux rises with the volume fraction of nano-copper oxide increases. Compared with the pure lithium bromide solution, as the temperature of cooling water at the inlet is in the range of 301.15 K to 307.15 K, the average mass transfer flux of the solution with 0.1% nanoparticles increases to about 1.33 times. Figure 11(b) shows that with the increase of the temperature of cooling water at the inlet, the value of the mass transfer enhancement factor is almost unchanged. Therefore, the effect of the temperature of cooling water at the inlet on mass transfer enhancement factor is not obvious.

5. Conclusions

In this paper, the finite element method was used to establish a thermal-mass coupling model for LiBr solution falling film absorption. The influence of nano-copper oxide on the falling film absorption of LiBr solution was investigated. The following conclusions are drawn.

(1) For the falling film absorption of pure lithium bromide solution, as the film flow rate grows, the average mass flux rises first and then decreases. When the film flow rate is too large or too small, it is not conducive to the absorption process, and there is an optimum film flow rate.

(2) Reducing the temperature of solution at the inlet, increasing the concentration of solution at the inlet or decreasing the temperature of cooling water at the inlet is beneficial to the mass transfer process.

(3) The mass transfer flux rises rapidly near the inlet and reaches the maximum, then reduces. The mass transfer coefficient of liquid phase decreases rapidly after reaching the maximum near the inlet, and tends to be stable as the downstream distance increases.

(4) After adding copper oxide nanoparticles into lithium bromide solution, mass transfer flux, mass transfer rate and mass transfer coefficient are all increased.

(5) When the temperature of solution at the inlet is high and the concentration of solution at the inlet is low, the improvement of the nano-copper oxide is more significant.

Acknowledgments

This work was financially supported by National Natural Science Foundation of China (No. 50976015), Research funds of the Maritime Safety Administration of the People's Republic of China (2012_27), and the Fundamental Research Funds for the Central Universities (3132019305).

References

[1] Ashrafmansouri, S. S., and Esfahany, M. N., Mass transfer in nanofluids: A review. *International Journal of Thermal Sciences,*82 (2014), 84-99.

[2] Krishnamurthy, S., Bhattacharya, P., Phelan, P.E., et al, Enhanced Mass Transport in Nanofluids. *Nano Letters,* 6(2006), 419-423.

[3] Pang, C., Wu, W., Sheng, W., et al, Mass Transfer Enhancement by Binary Nanofluids (NH3/H2OAg Nanoparticles) for Bubble Absorption Process, *International Journal of Refrigeration,* 35(2012), 2240–2247.

[4] Khan, W. A., and Gorla, R. S. R., Heat and Mass Transfer in Power-Law Nanofluids Over a Non-isothermal Stretching Wall With Convective Boundary Condition, ASME Journal of Heat Transfer, 134(2012), 112001.

[5] Chen, T., Kim, J., Cho, H. H., Theoretical Analysis of the Thermal Performance of a Plate Heat Exchanger at Various Chevron Angles Using Lithium Bromide Solution With Nanofluid, International Journal of Refrigeration, 48(2014), 233–244.

[6] Heris, S. Z., Etemad, S. G., Esfahany, M. N., Experimental investigation of oxide nanofluids laminar flow convective heat transfer. International Communications in Heat and Mass Transfer, 33(2006), 529-535.

[7] Kang, Y. T., Kim, H. J., Lee, K. I., Heat and mass transfer enhancement of binary nanofluids for H2O/LiBr falling film absorption process. International Journal of Refrigeration, 31(2008), 850-856.

[8] Kim, J. K., Jung, J. Y., Kang, Y. T., The effect of nano-particles on the bubble absorption performance in a binary nanofluid. International Journal of Refrigeration, 29(2006), 22-29.

[9] Yang, L., Du, K, Niu, X. F., et al. Experimental study on enhancement of ammonia–water falling film absorption by adding nano-particles. International Journal of Refrigeration, 34(2011), 640-647.

[10] Li, Y. J., Du, K., Jiang, W. X., Mechanism analysis on performance enhancement of ammonia-water falling film generation by nanofluid. Refrigeration, 44(2016), 51-57.

[11] Armou, S., Mir, R., El, H. Y., et al, Heat and Mass Transfer Enhancement in Absorption of Vapor in Laminar Liquid Film by Adding Nano-Particles. Journal of Applied Fluid Mechanics, 10 (2017),1711-1720.

[12] Wang, G., Zhang, Q., Zeng, M., et al. Investigation on mass transfer characteristics of the falling film absorption of LiBr aqueous solution added with nanoparticles. International Journal of Refrigeration, 89(2018), 149-158.

[13] Zhang, L. Y., Li, Y., Wang, Y., et al. Effect of Nanoparticles on H2O/LiBr Falling Film Absorption Process. ASME 2016 5th International Conference on Micro/Nanoscale Heat and Mass Transfer. American Society of Mechanical Engineers, 2016, 1-11.

[14] Moghadassi, A., Ghomi, E., Parvizian, F., A Numerical Study of Water Based Al2O3and Al2O3–Cu Hybrid Nanofluid Effect on Forced Convective Heat Transfer, International Journal of Thermal Sciences, 92(2015), 50–57.

[15] Khanolkar, R.U., and Suresh, A. K., Enhanced Mass Transfer Rates in Nanofluids: Experiments and Modeling, ASME Journal of Heat Transfer, 137(2015),091008.

[16] Karami S, Farhanieh B. A numerical study on the absorption of water vapor into a film of aqueous LiBr falling along a vertical plate. Heat and Mass Transfer, 46(2009), 197-207.

[17] Gao, H. T., and Hihara E., Surface Tension of LiBr Aqueous Solution with Heat Mass Transfer Enhancement Additives. Journal of Refrigeration, 3(2004), 5-8.

[18] Niu, X. F., Kai, D., Du, S. X., Numerical analysis of falling film absorption with ammonia–water in magnetic field. Applied Thermal Engineering, 27(2007), 2059-2065.

[19] Chang, H. C., and Demekhin, E. A., Complex Wave Dynamics on Thin Films. Netherlands: Elsevier Press, (2002).

[20] Brinkman, H. C., The viscosity of concentrated suspensions and solutions. Journal of Chemical Physics. 20(1952), 571-581.

[21] Xuan, Y. and Roetzel, W., Conceptions for heat transfer correlation of nanofluids. International Journal of Heat and Mass Transfer, 43(2000), 3701-3707.

[22] Pak, B.C., and Cho, Y. I., Hydrodynamic and heat transfer study of dispersed fluids with submicron metallic oxide particles. Experimental Heat Transfer, 11(1998),151-170.

[23] Celik I B, Ghia U, Roache P J, et al. Procedure for estimation and reporting of uncertainty due to discretization in CFD applications [J]. Journal of Fluids Engineering, 130(2008), 078001.

List of Figures

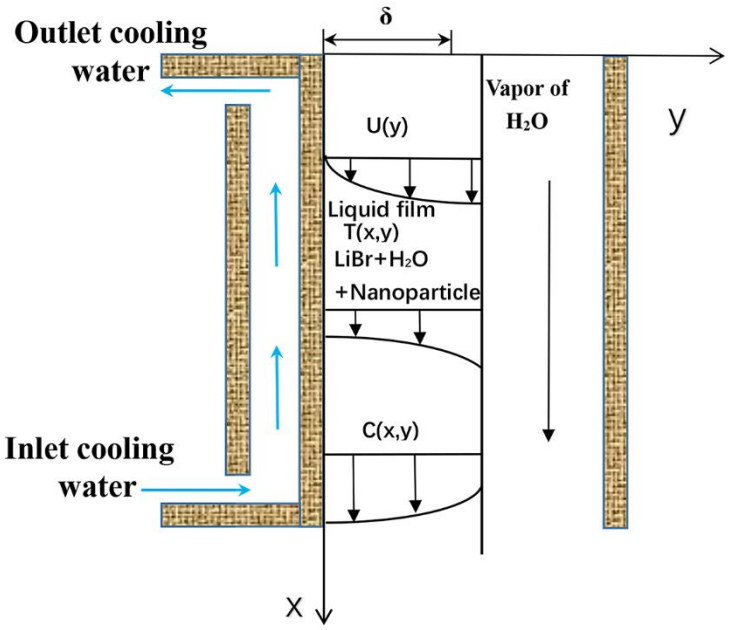

Fig 1. 2D model of the absorption process

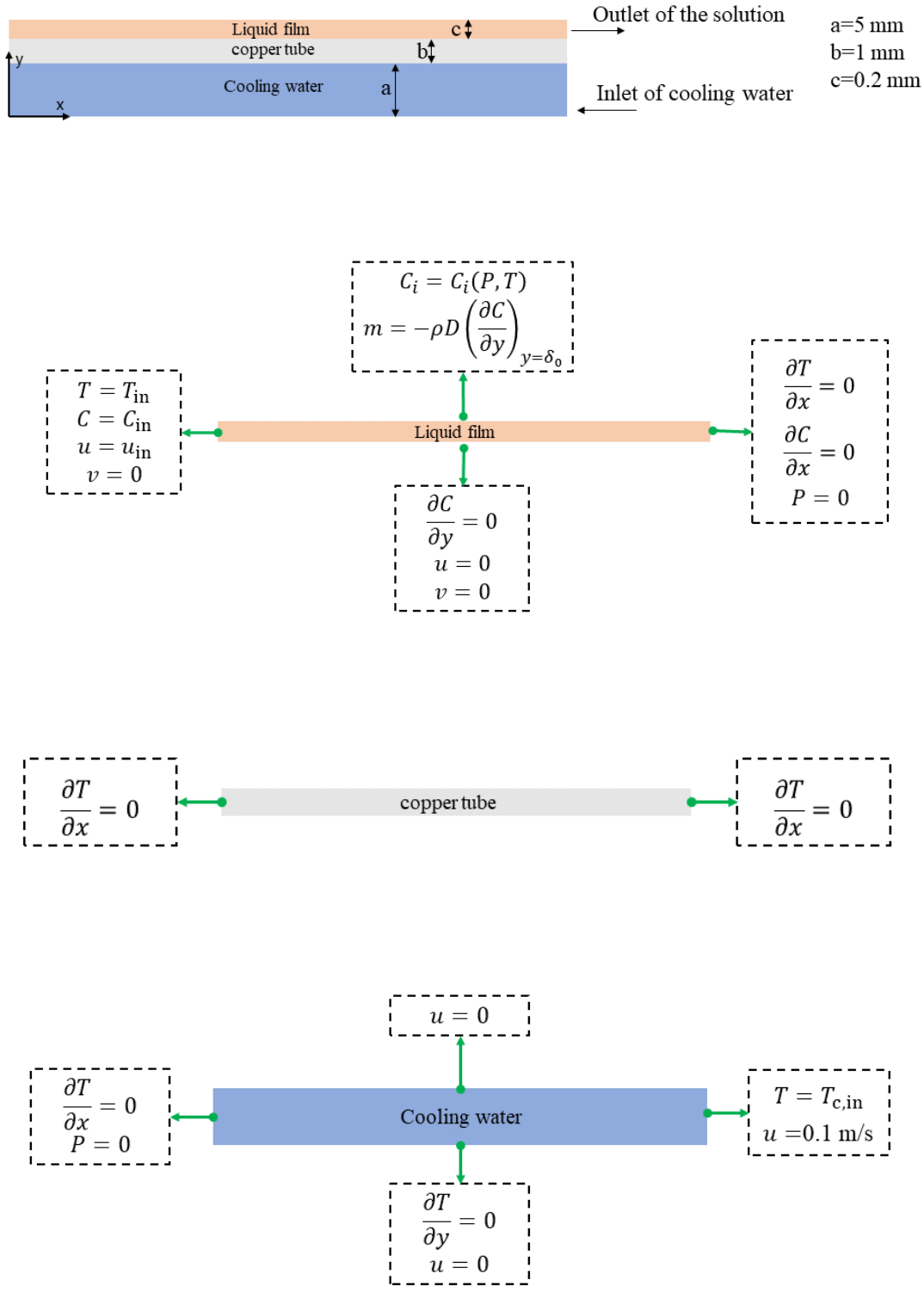

Fig.2 Boundary conditions

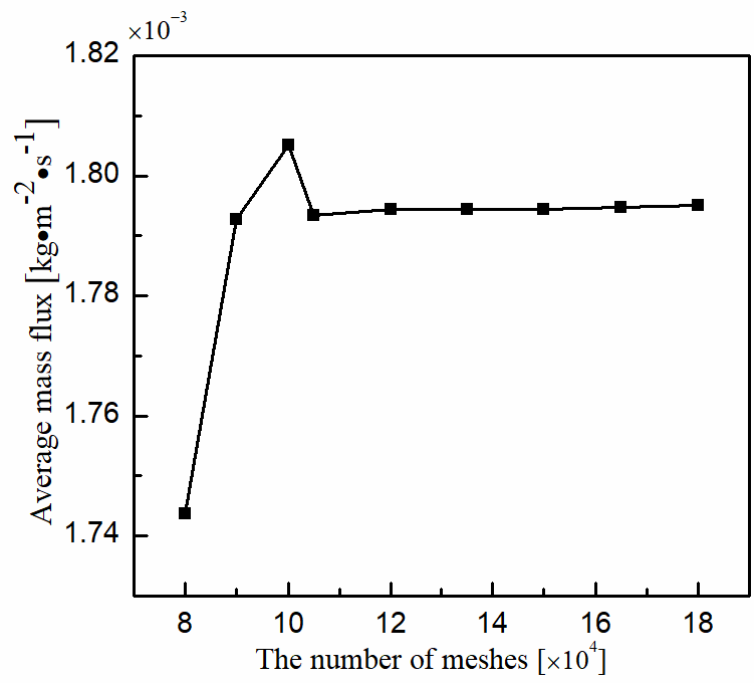

Fig.3 Grid verification

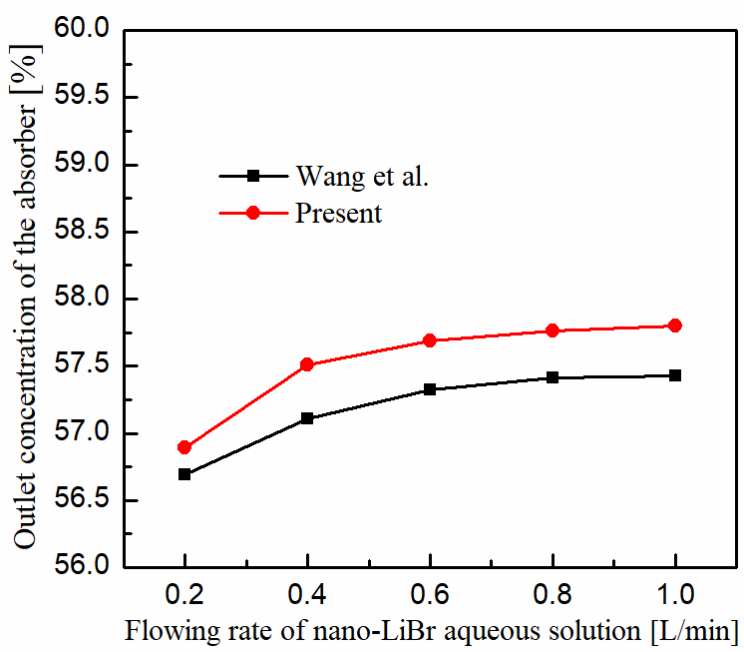

Fig.4 Comparison of our numerical results with experimental results (Wang et al)

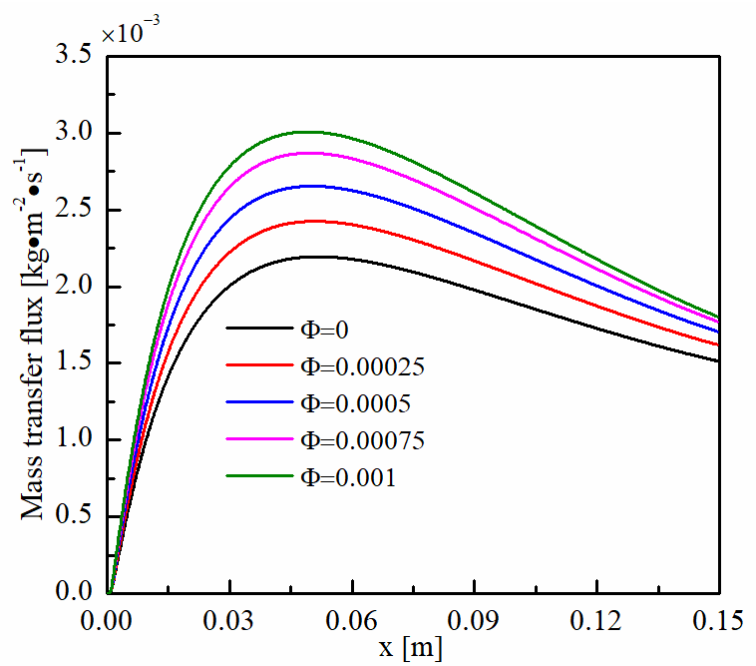

Fig.5 Variation of mass transfer flux with volume fraction of nanoparticles

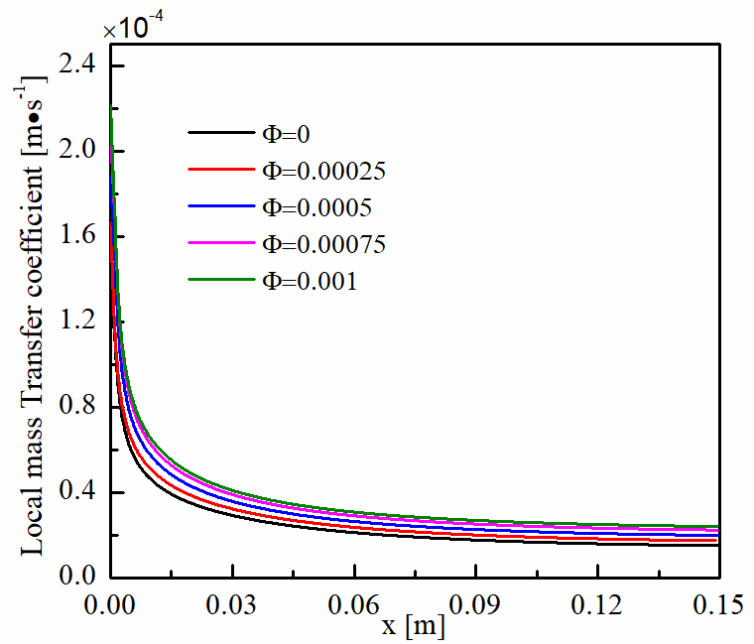

Fig.6 Variation of mass transfer coefficient in liquid phase with volume fraction of nanoparticles

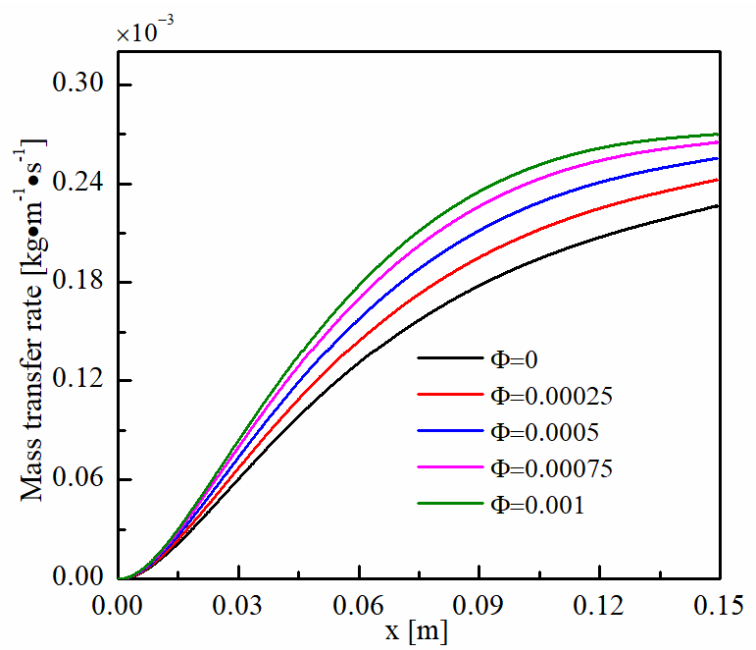

Fig.7 Variation of mass transfer rate with volume fraction of nanoparticles

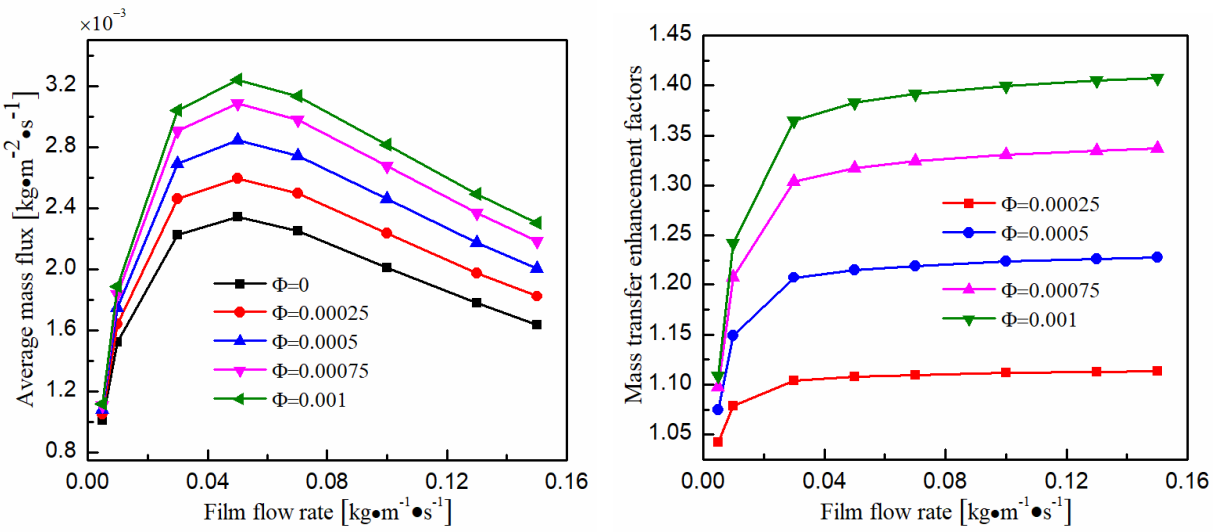

(a) Average mass transfer flux (b) Mass transfer enhancement factors

Fig.8 Film flow rate and different volume fractions of CuO nanoparticles

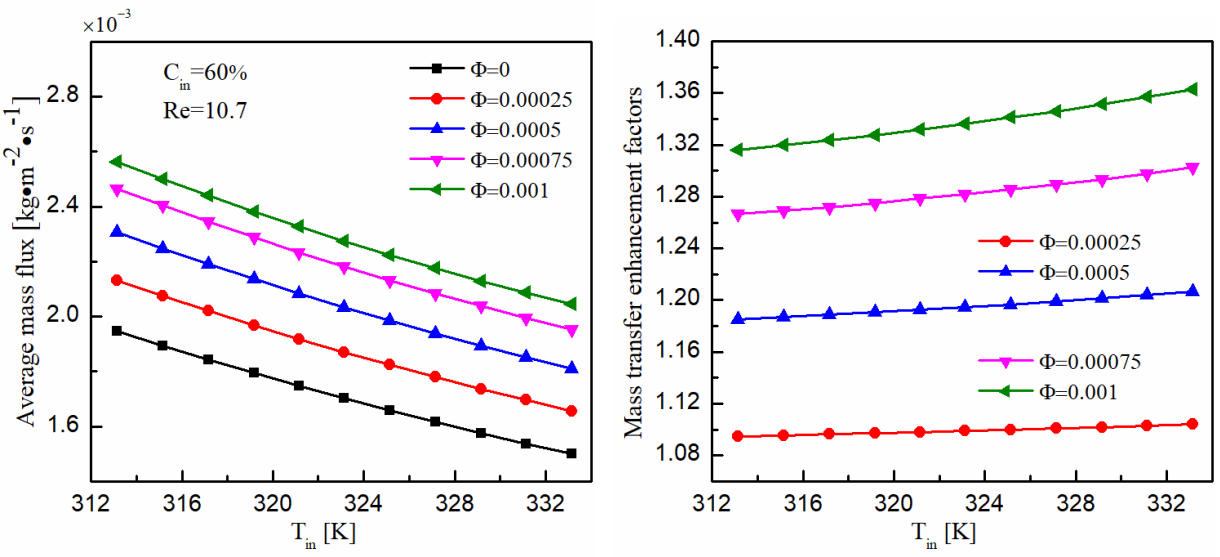

(a) Average mass transfer flux (b) Mass transfer enhancement factors

Fig.9 Solution inlet temperature and different volume fractions of CuO nanoparticles.

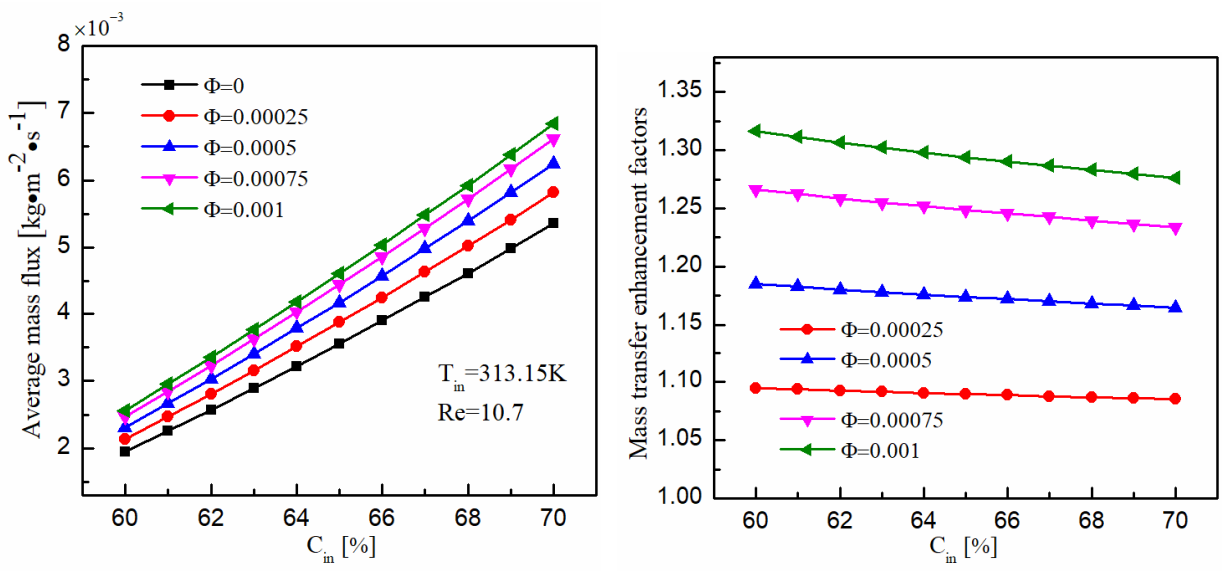

(a) Average mass transfer flux (b) Mass transfer enhancement factors

Fig.10 Solution inlet concentration and different volume fractions of CuO nanoparticles.

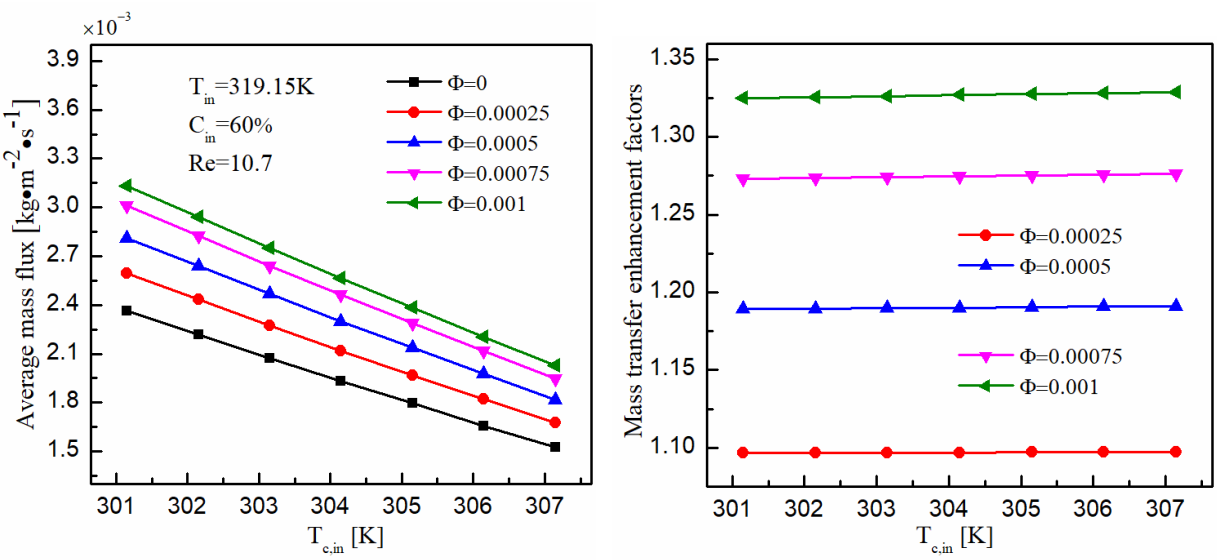

(a) Average mass transfer flux (b) Mass transfer enhancement factors

Fig.11 Cooling water inlet temperature and different volume fractions of CuO nanoparticles.

List of Tables

Table 1. Details of mesh size.

Case	Meshes
Fine	180000
Medium	135000
Coarse	80000

Table 2. Mesh sensitivity analysis

Case	ID	Meshes	m
Fine	ϕ_1	180000	1.7944×10^{-3}
Medium	ϕ_2	135000	1.7927×10^{-3}
Coarse	ϕ_3	80000	1.7136×10^{-3}
R_G	-	-	0.021491783

Table 3. Calculation of the discretization error for mass transfer flux

Item	m
r_{21}	1.2
r_{32}	1.29
ϕ_1	0.17944
ϕ_2	0.17927
ϕ_3	0.17136
p	14.24
ϕ_{ext}^{21}	1.79
e_a^{21}	0.095%
e_{ext}^{21}	0.014%
GCI_{fine}^{21}	0.018%

Table 4. Operating conditions.

Parameters	Value
Solution inlet concentration	60%
Solution inlet temperature	319.65K
System pressure	1 kPa
Length of falling film	150mm
Cooling water inlet temperature	305.15K
Cooling water channel height	5mm
Cooling water inlet velocity	0.1m/s